

Gap and embedded solitons in microwave-coupled binary condensates

Zhiwei Fan¹, Zhaopin Chen¹, Yongyao Li^{1,2} and Boris A. Malomed^{1,3}

¹*Department of Physical Electronics, School of Electrical Engineering,
Faculty of Engineering, Tel Aviv University, Tel Aviv 69978, Israel*

²*School of Physics and Optoelectronic Engineering, Foshan University, Foshan 528000, China*

³*Center for Light-Matter Interaction, Tel Aviv University, Tel Aviv 69978, Israel*

It was recently found that, under the action of the spin-orbit coupling (SOC) and Zeeman splitting (ZS), binary BEC with intrinsic cubic nonlinearity supports families of gap solitons, provided that the kinetic energy is negligible in comparison with the SOC and ZS terms. We demonstrate that, also under the action of SOC and ZS, a similar setting may be introduced for BEC with two components representing different atomic states, resonantly coupled by microwave radiation, while the Poisson's equation accounts for the feedback of the two-component atomic wave function onto the radiation. The microwave-mediated interaction induces an effective nonlinear trapping potential, which strongly affects the purport of the linear spectrum in this system. As a result, families of both gap and *embedded* solitons (those overlapping with the continuous spectrum) are found, which are chiefly stable. The shape of the solitons features exact or broken skew symmetry. In addition to fundamental solitons (whose shape may or may not include a node), a family of dipole solitons is constructed too, which are even more stable than their fundamental counterparts. A nontrivial stability area is identified for moving solitons in the present system, which lacks Galilean invariance. Colliding solitons merge into a single one.

I. INTRODUCTION

The realization of the spin-orbit coupling (SOC) in quantum atomic gases [1]-[6] and exciton-polariton condensates in semiconductor microcavities [7]-[13] has initiated a new direction in experimental and theoretical studies of atomic and photonic waves. While SOC is a linear effect, its interplay with intrinsic nonlinearity of Bose-Einstein condensates (BECs) makes it possible to predict the creation of topological modes in these settings, such as vortices [14], monopoles [16], and skyrmions [17, 18], as well as stable one-dimensional [19]-[25], two-dimensional [26]-[31], and three-dimensional [32] solitons, see also a brief review in Ref. [33].

A specific approach to the creation of stable one- and two-dimensional solitons in two-component BEC subject to the combined action of SOC and Zeeman splitting (ZS), which is a generic ingredient of SOC systems [34], was recently proposed in Refs. [30] and [57], under the condition that the SOC and ZS terms in the system's Hamiltonian are much larger than the kinetic energy. Neglecting, accordingly, the second derivatives in the respective system of coupled Gross-Pitaevskii equations (GPEs), which include the combination of the SOC and ZS terms, one obtains a linear spectrum with a finite bandgap. The cubic nonlinearity induced by atomic collisions in BEC may readily create families of solitons populating the bandgap. In this connection, it is relevant to mention that gap solitons were predicted [40-42] and experimentally demonstrated [43, 44] in fiber-optic Bragg gratings, in polariton condensates under the action of photonic lattices [45, 46], and in the single-component BEC loaded in an optical-lattice potential [47-49].

The consideration of such models (they may be loosely defined as those for "heavy atoms", whose kinetic energy may be omitted) is relevant because, as it was shown in Ref. [30], if a low-dimensional SOC system is derived from the three-dimensional one, being subject to the action of tight confinement in the transverse direction(s), the kinetic energy in the ensuing system of GPEs is indeed much smaller than the energies corresponding to the SOC terms. The possibility to omit the terms with the second derivatives also plays a crucial role in the context of BEC systems with a flatband spectrum [50].

Another relevant setting for the interplay of SOC and nonlinearity is offered by the system composed of hyperfine atomic states resonantly coupled by the magnetic component of the microwave radiation, with the feedback of the atomic states on the radiation governed by the corresponding Poisson's equation [51]. This system gives rise to hybrid matter-wave-microwave solitons (somewhat similar, in this respect, to exciton-polariton solitons in semiconductor microcavities [45, 46, 52]). The SOC was recently added to this model in Ref. [35]. The aim of the present work is to transform the system into one dominated by the first-order spatial derivatives, accounting for the SOC, and produce families of stable solitons in the system. An essential peculiarity of the setting is that the effectively nonlocal interaction between the components, mediated by the microwave field, strongly affects the concept of the linear spectrum, by adding an effective nonlinear trapping potential to the linearized system, see Eq. (9) below. In other words, the nonlocal nonlinearity makes the system *non-linearizable*, and alters the fundamental significance of the bandgap. As a result, the system generates, depending on the relative strength of contact and microwave-induced nonlinear terms, families of gap solitons, as well as families of *embedded* solitons [53]-[56], which exist inside the

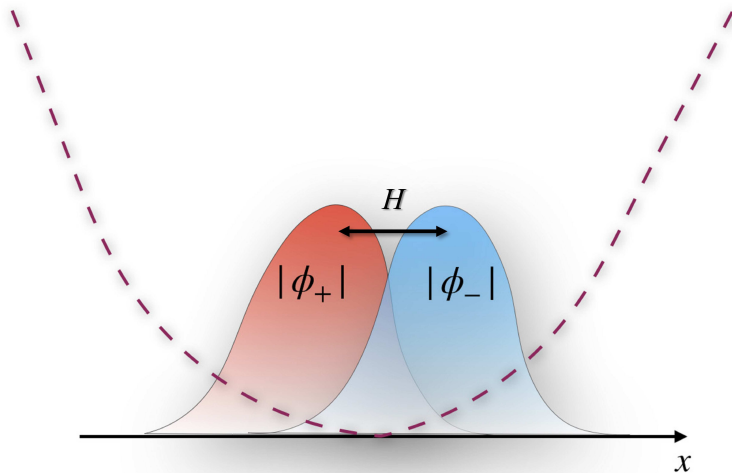


FIG. 1: A sketch of the system composed of the binary Bose-Einstein condensate, with components (ϕ_+, ϕ_-) , trapped in the effective nonlinear potential (shown by the dashed curve) induced by the microwave-mediated interaction, and linearly coupled by the effective Rabi mixing $\sim H$, designated by the double arrow (\leftrightarrow). The sketch shows the shape of a typical skew-symmetric soliton (the ZS will break the mutual symmetry of the two components).

radiation band, while the bandgap remains empty. Another noteworthy findings is that, on the contrary to what is commonly known about ground states in linear settings, in the present nonlinear system fundamental solitons, which realize the ground state, may feature a node (zero crossing) in their profile. In addition to the fundamental modes, we also find stable excited states in the form of dipole solitons. Interestingly, their stability area is *broader* than the one for the fundamental counterparts. A stability area is also identified for moving fundamental solitons, which is a nontrivial finding for the present system, which is not subject to the Galilean invariance. Interaction between counterpropagating solitons leads to multiple collisions and eventual merger.

The main part of the paper is organized as follows. The model and some analytical results are formulated in Section II. Numerical findings for fundamental and dipole solitons, as well as for moving ones, are summarized in Section III. The paper is concluded by Section IV.

II. THE MODEL

The binary BEC, with two components $\phi_{\pm}(x, t)$ of the mean-field wave function coupled linearly by SOC and nonlinearly by the microwave radiation, is modeled by a system of one-dimensional GPEs. In a scaled form, the system, in which the kinetic-energy terms are neglected (as said above), is written, following Ref. [35] (in which the kinetic energy was kept), as

$$\begin{aligned} i\partial_t\phi_+ &= \partial_x\phi_- - \Omega\phi_+ - H\phi_- - g|\phi_+|^2\phi_+ + \frac{\gamma}{2}\phi_- \int_{-\infty}^{+\infty} |x-x'|\phi_-^*(x')\phi_+(x')dx', \\ i\partial_t\phi_- &= -\partial_x\phi_+ + \Omega\phi_- - H\phi_+ - g|\phi_-|^2\phi_- + \frac{\gamma}{2}\phi_+ \int_{-\infty}^{+\infty} |x-x'|\phi_-(x')\phi_+^*(x')dx', \end{aligned} \quad (1)$$

where $*$ stands for the complex-conjugate expression. Here, the coefficient of SOC, represented by the x -derivatives, is scaled to be 1, Ω is the ZS strength, which may be imposed by dc magnetic field (alternatively, the same terms may be represent the Stark - Lo Surdo effect, imposed by dc electric field), the amplitude of the magnetic component of the background microwave field is H (in fact, it induces an effective Rabi mixing in the system, cf. Refs. [31, 36–38]), and

the contact self-interaction in each component (if any) is represented by coefficient g ($g > 0$ and $g < 0$ correspond to self-attraction and repulsion, respectively). Contact cross-interaction between the components can be readily added to the system, in the form of terms $\sim |\phi_{\mp}|^2 \phi_{\pm}$ in each equation, but they do not produce essential changes in the results reported below. The integral terms represent the feedback of the microwave field, generated by transitions between the ϕ_{\pm} components, with strength $\gamma > 0$, on these components. By means of rescaling admitted by Eq. (1), we set $\gamma = 0.5$ and $\Omega = 1$, unless $\Omega = 0$ (in Ref. [35], different scaling was adopted, with $\gamma = 0.02$). The integral terms are actually generated by the solution of the respective one-dimensional Poisson equation, written in terms of the corresponding Green's function, $G(x, x') = (1/2)|x - x'|$ [35]. A schematic of the system under the consideration is displayed in Fig. 1.

Stationary states with chemical potential μ are looked for as solutions to Eq. (1) in the form of

$$\phi_{\pm} = \exp(-i\mu t)u_{\pm}(x), \quad (2)$$

with real stationary wave functions u_{\pm} obeying the following integro-differential equations:

$$\begin{aligned} \mu u_+ &= \partial_x u_- - \Omega u_+ - H u_- - g u_+^3 + \frac{\gamma}{2} u_- \int_{-\infty}^{+\infty} |x - x'| u_-(x') u_+(x') dx', \\ \mu u_- &= -\partial_x u_+ + \Omega u_- - H u_+ - g u_-^3 + \frac{\gamma}{2} u_+ \int_{-\infty}^{+\infty} |x - x'| u_-(x') u_+(x') dx'. \end{aligned} \quad (3)$$

Note that, in the absence of the ZS, $\Omega = 0$, Eq. (3) admits the *skew-symmetry* reduction,

$$u_+(x) = \pm u_-(-x), \quad (4)$$

which is broken by the ZS terms.

Equations (1) conserve the total norm,

$$N \equiv \int_{-\infty}^{+\infty} (|u_+(x)|^2 + |u_-(x)|^2) dx, \quad (5)$$

and energy (Hamiltonian),

$$\begin{aligned} E &= \int_{-\infty}^{+\infty} dx \left[\phi_+^* \partial_x \phi_- - \phi_-^* \partial_x \phi_+ + \Omega (|\phi_-|^2 - |\phi_+|^2) - H (\phi_+^* \phi_- + \phi_-^* \phi_+) \right. \\ &\quad \left. - \frac{g}{2} (|\phi_+|^4 + |\phi_-|^4) \right] + \frac{\gamma}{2} \int_{-\infty}^{+\infty} \int_{-\infty}^{+\infty} |x - x'| dx dx' [\phi_+^*(x) \phi_-(x) \phi_-^*(x') \phi_+(x')]. \end{aligned} \quad (6)$$

Note that, with regard to the possibility of the integration by parts, expression (6) is real, even if the SOC terms in the integrand seem complex.

The linearization of Eq. (3) produces the dispersion relation in the free space (in the absence of an external trapping potential),

$$\mu^2 = \Omega^2 + H^2 + k^2, \quad (7)$$

which demonstrates that the background magnetic field and ZS contribute to the formation of the spectral gap,

$$-\sqrt{\Omega^2 + H^2} < \mu < +\sqrt{\Omega^2 + H^2}, \quad (8)$$

in which one may expect the creation of gap solitons under the action of the system's nonlinearities, cf. Refs. [30] and [57]. The gap is located between semi-infinite bands populated by radiation modes. Nevertheless, it is shown below that, in addition to the in-gap solitons, the system readily creates families of *embedded solitons* in the bands, while the gap is left empty. This finding can be readily understood, as Eq. (3) takes the following asymptotic form at $|x| \rightarrow \infty$:

$$\begin{aligned} \mu u_+ &= \partial_x u_- - \Omega u_+ - H u_- + \frac{\gamma}{2} I |x| u_-, \\ \mu u_- &= -\partial_x u_+ + \Omega u_- - H u_+ + \frac{\gamma}{2} I |x| u_+. \end{aligned} \quad (9)$$

where

$$I \equiv \int_{-\infty}^{+\infty} u_-(x')u_+(x')dx \quad (10)$$

is a constant. The effective cross-potential in Eq. (9), growing $\sim |x|$ at $|x| \rightarrow \infty$, completely changes the definition of the system's spectrum, and may make the distinction between the gap and bands, predicted by the linearization of the system, irrelevant. Indeed, the asymptotic form of the solution to Eq. (9) is

$$\begin{aligned} \{u_-(x), u_+(x)\} &\approx u_0^{(-)} \left\{ 1, \frac{\mu - \Omega}{\gamma I} x^{-1} \right\} \exp\left(-\frac{\gamma}{4}|I|x^2\right) \text{ at } x \rightarrow +\infty, \\ \{u_+(x), u_-(x)\} &\approx u_0^{(+)} \left\{ 1, \frac{\mu + \Omega}{\gamma I} |x|^{-1} \right\} \exp\left(-\frac{\gamma}{4}|I|x^2\right) \text{ at } x \rightarrow -\infty, \end{aligned} \quad (11)$$

where $u_0^{(\mp)}$ are constants. In the case of $\Omega = 0$, this solution has $u_0^{(-)} = -u_0^{(+)}$, satisfying the skew-symmetry condition (4) with the bottom sign [the particular sign is selected by comparison with the full numerical solution (3)].

The Gaussian asymptotic form produced by Eq. (11) is drastically different from the exponential expressions for tails of ordinary gap solitons, which explains the possibility of finding soliton families in the band, rather than in the gap, as shown below by numerically found solutions. In fact, the asymptotic form (9) implies that the underlying GPE system (1) is *non-linearizable*, cf. Ref. [39]. Comparison between numerical solutions and analytical prediction given by Eq. (11) is also shown below, in Fig. 7.

III. NUMERICAL RESULTS

A. Fundamental solitons

Soliton solutions of Eq. (3) were produced by means of the squared-operator iteration method [58]. Then, their stability or instability was identified by means of direct simulations of the perturbed evolution.

First, in Figs. 2(a,b,c) and (d,e,f) we display, severally, typical examples of stationary wave functions $u_{\pm}(x)$ for skew-symmetric and asymmetric solitons. All these solutions may be identified as ground states. In particular, the modes shown in panels (a,b,d,e) comply with the fundamental principle, borrowed from linear theories, which states that ground-state profiles must not have zero-crossing points (nodes). Nevertheless, the ground states presented in panels (c) and (f) break this principle, each featuring one node, which may be possible in nonlinear systems [in the present case, the nodes emerge if the relatively strong self-attraction terms, with $g = 1$, are present in Eq. 1)]. It is relevant to note that, in the absence of the background magnetic field ($H = 0$), the ground state of the SOC system takes the form of the gap soliton, with one spatially even nodeless component, and the other odd one, which has the node at the center [57]. Accordingly, the nodes observed in Figs. 2(c) and (f) may be considered as ‘‘remnants’’ of the nodes in the above-mentioned odd component. The solitons with nodes, displayed in (c) and (f), are identified as ground states, as they belong to families which are produced by continuation of ones representing nodeless ground-state solitons – for instance, the blue and green lines in Figs. 3(c) and (f) are obtained as continuous extensions of the red and violet segments. No nodeless modes could be found for those values of N at which the noded ground-state solitons have been produced by the solution of Eq. (3).

A natural trend, demonstrated by the comparison of different profiles in Fig. 2, is that the transition from the self-repulsion to attraction, i.e., from $g < 0$ to $g > 0$, leads to compression of each component. Further, the two components generate each other linearly via the SOC and Rabi coupling (the latter one represented by H), and simultaneously they mutually repel nonlinearly, through the effective cross-potentials $\sim \gamma$ in Eq. (9). Accordingly, the self-compressed components with larger amplitudes stronger repel each other, featuring effective separation in Figs. 2(c,f). Finally, the strong separation makes coefficient $|I|$ (10) smaller, which weakens the role of the effective confining potentials in Eqs. (9) and (11) in comparison with the linear SOC and Rabi terms in the asymptotic area, $|x| \rightarrow \infty$, thus allowing the solitons to populate the linearly-predicted gap, as seen below in Figs. 3(c,f).

Systematic results, including the location of families of the skew-symmetric and asymmetric solitons with respect to the bandgap (8), and their stability, are summarized in Fig. 3, by means of $\mu(N)$ dependences for the soliton families in six generic cases. Only in panels (c) and (f) these are families of in-gap solitons. In other cases they exist, as embedded solitons, in radiation bands, while the gap remains empty. Embedded solitons were not found in Ref. [57], while families of gap solitons obtained in the model with the dipole-dipole interaction, considered in Ref. [30], extend into the bands (however, gaps were never empty in that system).

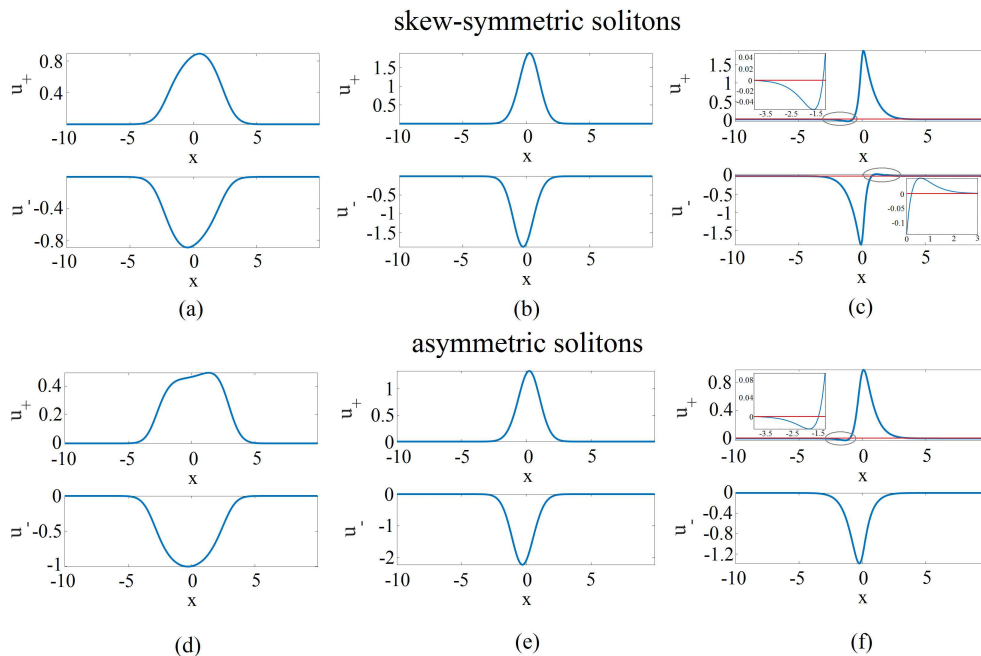


FIG. 2: Panels (a,b,c) and (d,e,f) display typical examples of ground-state soliton profiles which are, respectively, skew-symmetric (with $\Omega = 0$) and asymmetric (with $\Omega = 1$). The other parameters are $\gamma = 0.5$ and (a) $(N, H, g) = (5, 1, -1)$, belonging to the magenta line in Fig. 3(a); (b) $(N, H, g) = (10, 1, 0)$, belonging to the blue line in Fig. 3(a); (c) $(N, H, g) = (5, 1, 1)$, belonging to the red line in Fig. 3(c); (d) $(N, H, g) = (5, 1, -1)$, belonging to the orange line in Fig. 3(d); (e) $(N, H, g) = (10, 1, 0)$, belonging to the green line in Fig. 3(d); (f) $(N, H, g) = (3, 1, 1)$, belonging to the violet line in Fig. 3(f). A nontrivial feature, observed in the in-gap solitons in panels (c) and (f), is that a sufficiently strong contact self-attraction, with $g = 1$, creates *zero-crossings* (nodes) in the ground-state profiles. The nodes are clearly shown in insets to panels (c) and (f), which zoom the wave-function profiles in regions denoted by gray circles in the main plots. Other solitons [shown in panels (a), (b), (d), and (e)] are embedded (in-band) ones, which are free of nodes. The soliton in (c) is unstable, all other ones being stable.

It is worthy to note that the Vakhitov-Kolokolov (VK) [58–60] or anti-VK [61] criteria, which relate the sign of the slope, $d\mu/dN < 0$ or $d\mu/dN > 0$, to the necessary stability condition for solitons which are supported, severally, by the self-attractive or repulsive nonlinearities, is valid in the present system when both the nonlocal and local nonlinearities are self-repulsive. Indeed, in Figs. 3(a,d), the families satisfy the anti-VK criterion, $d\mu/dN > 0$, and are indeed completely stable. On the other hand, it is not surprising that, in the case when the solitons are supported by the combination of the nonlocal repulsion and contact attraction, the VK/anti-VK criterion does not hold, as it is not possible to identify the dominant nonlinear term: in Figs. 3(b,e), the change of the sign from $d\mu/dN > 0$ to $d\mu/dN < 0$ does not lead to destabilization of the solitons (non-compliance with the VK criterion occurs in other models too [58]). As concerns the evolution of unstable solitons and interaction between stable ones, they are similar to examples displayed below in Figs. 6(b) and (c).

In the case of $\Omega = 1$, results for the shape of the asymmetric fundamental solitons (nodeless or noded) and their stability are reported in Figs. 4 and 5, in the parameter plane of (H, N) , for different values of the contact-interaction constant, g . Panels (a) through (d) in Fig. 4 clearly demonstrate that the node appears in the stable ground-state soliton at $g \approx 0.2$, and the corresponding parameter area expands with the increase of g . Areas of stable and unstable solitons are also identified in Fig. 4. Additionally, the stability boundaries are displayed, for a set of positive and negative values of g , in Fig. 5. It is seen that the increase of the background magnetic field, i.e., Rabi coupling between the two components of the binary wave function, helps to stabilize the solitons. Generally, the increase of $|g|$ leads to destabilization, although in the case of the contact self-repulsion, $g < 0$, the situation is nearly opposite at $H < 0.3$.

Note that the stability maps displayed in Figs. 4 and 5 are plotted for $H \geq 0.1$. At smaller values of H , the solitons are very broad, being distorted by boundaries of the integration domain.

Next, we report systematic results produced for families of skew-symmetric solitons by the system without the ZS, $\Omega = 0$, in Fig. 6(a). In this case, $H = 1$ may be fixed by scaling, hence the full stability regions are displayed in the plane of (g, N) , including both positive and negative values of g . The plot clearly demonstrates monotonous shrinkage

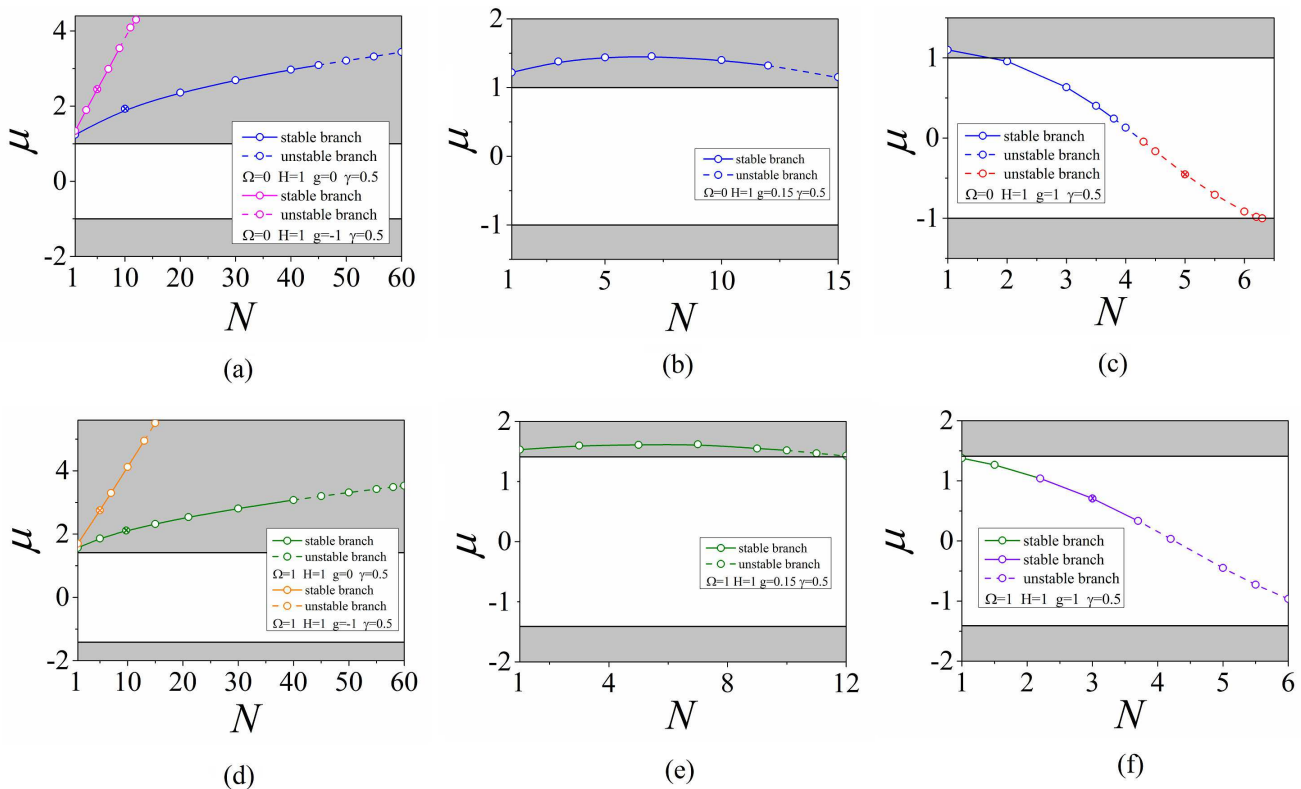


FIG. 3: Dependences $N(\mu)$ for six generic soliton families, at values of parameters indicated in panels. Solid and dashed lines represent stable and unstable segments of the families, respectively. In panels (c) and (f), red and violet lines (in the lower right) represent solitons with nodes, while blue and green ones (in the upper left) designate families of nodeless solitons. In each panel, white and gray areas represent, respectively, the bandgap, predicted by Eq. (8) for the linearized system, and the bands above and beneath the gap. Coordinates of points separating stable and unstable segments, as well as ones carrying nodeless and noded solitons, in different panels are: (a) $(N, \mu) = (9, 3.54)$ and $(45, 3.09)$; (b) $(N, \mu) = (12, 1.32)$; (c) $(N, \mu) = (3.8, 0.24)$ and $(N, \mu) = (4.3, -0.045)$ (this point separates the blue and red branches); (d) $(N, \mu) = (13, 4.95)$ and $(N, \mu) = (40, 3.08)$; (e) $(N, \mu) = (10, 1.52)$; (f) $(N, \mu) = (3.7, 0.33)$ and $(N, \mu) = (2.2, 1.04)$ (this point separates the green and violet branches). In panels (b) and (e) points corresponding to the largest values of μ are $(N, \mu) = (7, 1.46)$ and $(N, \mu) = (7, 1.62)$, respectively. In panels (a,c,d,f), examples of solitons shown in Fig. 2 are marked by cross-in-circle symbols.

of the stability area with the increase of $|g|$, which generally resembles the trend for asymmetric solitons, observed in Figs. 4 and 5 in the case of $\Omega = 1$.

Tails of the numerically found solitons indeed feature a Gaussian shape, as predicted by Eq. (11). The analytical prediction for the tails of a skew-symmetric soliton is compared to its numerically generated counterparts in Fig. 7(a), which demonstrates that the simple analytical approximation provides reasonable accuracy.

As concerns unstable solitons, direct simulations demonstrate that they are quickly destroyed, being replaced by a finite-amplitude turbulent state, as shown in Fig. 6(b) (the unstable evolution is similar in the case of $\Omega = 1$). Further, creating a pair of spatially separated solitons, it is natural to expect that the nonlocal interaction, mediated by the microwave field, will also induce a long-range interaction between non-overlapping solitons. This is indeed observed in Fig. 6(c), which demonstrates that the long-range interaction between the solitons destroys them, leading to creation of a quasi-linear interference pattern (which may be affected by reflections from edges of the integration domain, if the latter is not broad enough). A detailed study of interactions between solitons in the present system may be a subject for a separate work.

B. Dipole solitons

The above consideration addressed solely fundamental (ground-state) solitons. The fact that they are supported by the effective trapping potential in Eq. (9) suggests a possibility to look for higher-order solitons, that may correspond

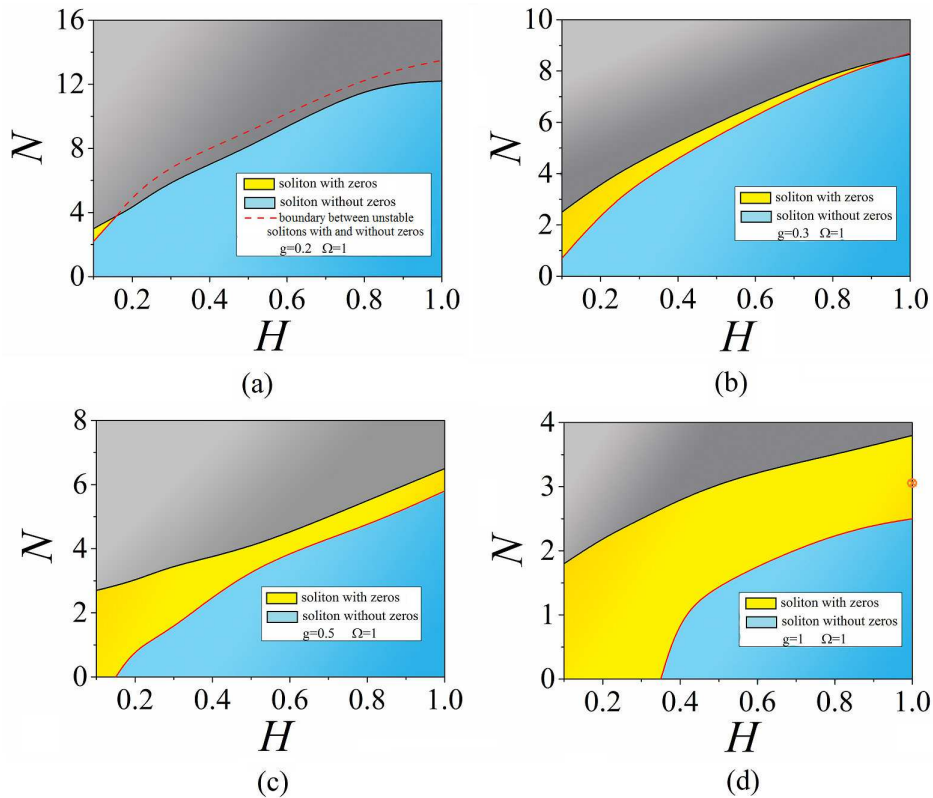


FIG. 4: Stability regions for asymmetric solitons in the parametric plane of (H, N) with $(\Omega, \gamma) = (1, 0.5)$. The solitons are unstable in the gray area (upper left), being stable as modes without and with intrinsic zero (node) in the blue (lower right) and yellow (middle) regions, respectively. In panel (a), unstable solitons in the stripe between the black and dashed red lines feature a node. The cross-in-circle symbol in panel (d) represents the stable soliton shown in Fig. 2(f).

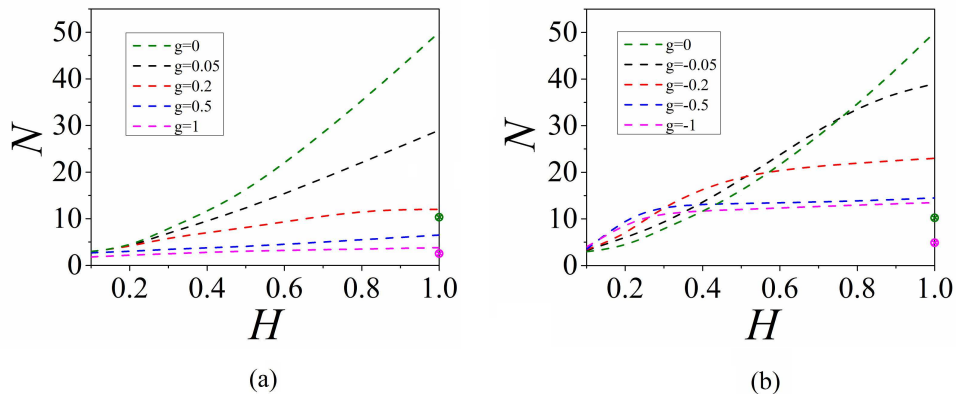


FIG. 5: Asymmetric solitons are stable beneath boundaries in the plane of (H, N) , displayed in this figure for $(\Omega, \gamma) = (1, 0.5)$, and a set of values of the self-interaction coefficient, corresponding to attraction [$g \geq 0$ in (a)] and repulsion [$g \leq 0$ in (b)]. The cross-in-circle symbols in panels (a) and (b) represent the stable solitons shown in Figs. 2(e,f) and (d,e), respectively. On the section $H = 1$, each line from the top to the bottom features the same order shown in the inset chart.

to excited bound states in the trapping potential (such stable states were not reported in related works [35], [30], and [57]; in the two latter papers, excited states were addressed, but they all were found to be unstable). The present system readily creates *stable* excited states in the form of dipole (spatially odd) modes, which, in the case of $\Omega = 0$, satisfy the skew-symmetry condition in the form of Eq. (4) with the top sign (on the contrary to the bottom sign corresponding to the fundamental states), as shown in Figs. 8(b) and 9(a,b) for the system without and with the contact interaction, *viz.*, $g = 0$ and $g = \pm 0.5$, respectively. Further, Figs. 8(a) and (b) compare the fundamental

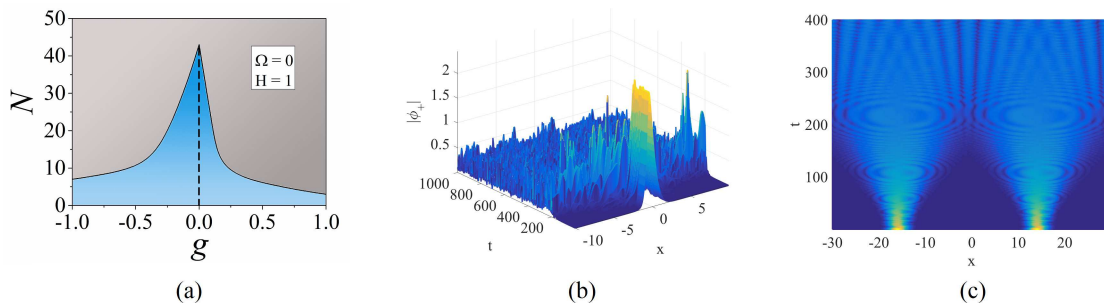


FIG. 6: In panel (a), skew-symmetric fundamental solitons are stable and unstable, respectively, in blue (bottom) and gray (top) areas in the plane of (g, N) , for fixed parameters $\Omega = 0$, $H = 1$, and $\gamma = 0.5$. (b) A typical example of the evolution of component ϕ_+ in an unstable soliton, with parameters $(N, \Omega, H, g, \gamma) = (8, 0, 1, 0.5, 0.5)$ (the instability is similar in the other component). (c) The simulation of the interaction between two identical stable solitons with phase shift $\Delta\varphi = 0$ between them. The parameters are $(N, \Omega, H, g, \gamma) = (10, 0, 1, 0, 0.5)$. The interaction is similar for other values of the phase shift, including $\Delta\varphi = \pi/2$ and π .

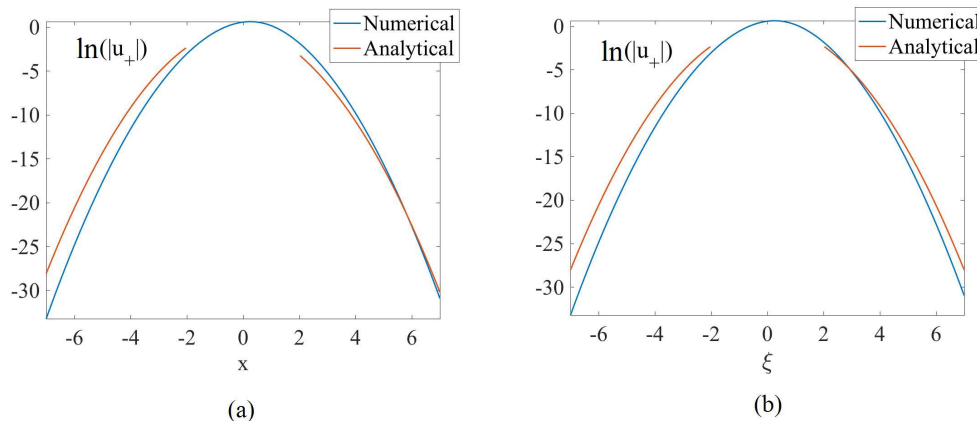


FIG. 7: The comparison between the logarithmic form of the analytically predicted Gaussian tails (red discontinuous lines) of the fundamental skew-symmetric solitons and their numerically found counterparts (blue continuous lines). (a) The comparison for a typical stable quiescent soliton with parameters $(N, \Omega, H, g, \gamma) = (10, 0, 1, 0, 0.5)$, the analytical prediction given by Eq. (11). (b) The comparison for a typical moving soliton, for $(N, \Omega, H, g, \gamma, v) = (10, 0, 1, 0, 0.5, 0.1)$, with the analytical prediction provided by Eq. (16). The comparison is displayed only for component u_+ , the pictures for u_- being mirror images of the present ones.

soliton and its dipole counterpart at identical values of the parameters, including the total norm (but, naturally, with different chemical potentials, $\mu_{\text{fund}} = 1.47$ and $\mu_{\text{dip}} = 1.91$), in the system with $g = 0$. The results are summarized in Fig. 8(c), which displays the $\mu(N)$ dependence for the family of stable skew-symmetric dipole solitons. Note that the family satisfies the anti-VK stability criterion, $d\mu/dN > 0$, which is relevant in this case, as the contact self-attraction is absent.

Next, Fig. 9(c) displays an example of a stable dipole mode in which the skew symmetry is broken by the ZS, with $\Omega = 1$. It is worthy to mention that, for the same parameters as used in the latter case, i.e., $(N, \Omega, H, g, \gamma) = (10, 1, 1, 0.3, 0.5)$, the fundamental soliton falls in the unstable (gray) area in Fig. 4(b), even if its chemical potential, $\mu_{\text{fund}} = 0.73$, is much smaller than $\mu_{\text{dip}} = 2.14$ of the stable dipole soliton with the same norm. Thus, the dipole solitons may be *more stable* than their fundamental counterparts, at the same parameters and with the same norm. To the best of our knowledge, no previous model produced a larger stability area for dipole solitons than for fundamental ones (in a specific model with spatially modulated nonlinearity, introduced in Ref. [39], the fundamental and dipolar solitons are completely stable in their entire existence area, while instability appears in higher-order excited states).

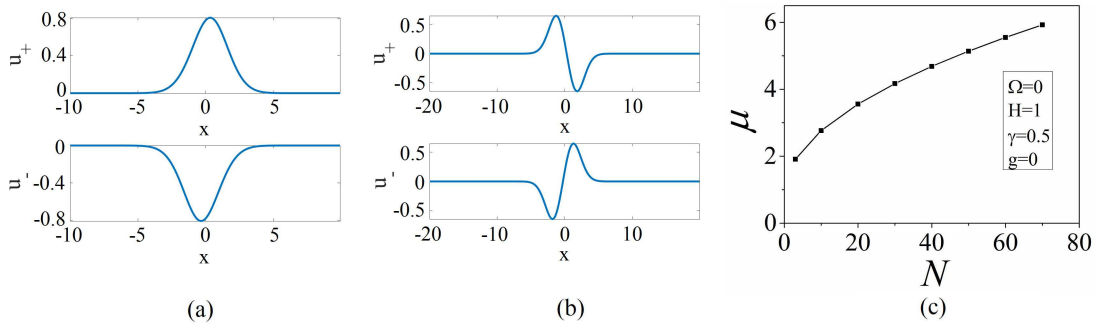


FIG. 8: (a) and (b): Examples of stable skew-symmetric fundamental and dipole solitons in the absence of the Zeeman splitting and contact nonlinearity, i.e., with $\Omega = 0$, $H = 1$, $g = 0$ and $\gamma = 0.5$, and equal norms, $N = 3$. The respective chemical potentials are $\mu_{\text{fund}} = 1.47$ and $\mu_{\text{dip}} = 1.91$. (c) Dependence $N(\mu)$ for the family of stable skew-symmetric dipole solitons.

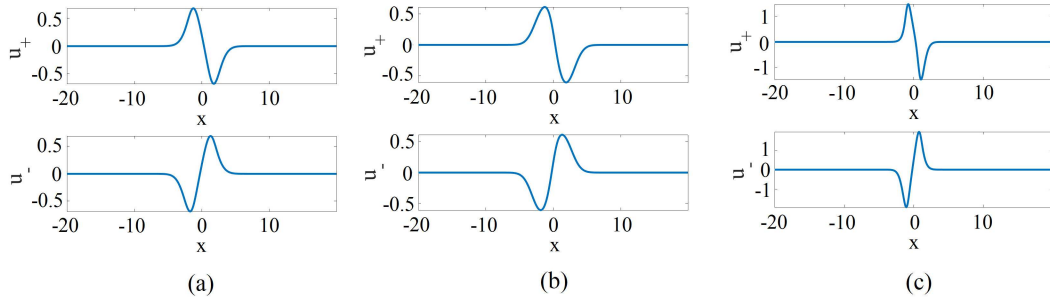


FIG. 9: (a,b) Typical examples of stable skew-symmetric dipole solitons in the system with $(\Omega, H, \gamma) = (0, 1, 0.5)$, which includes the contact self-attraction and repulsion, respectively, with $g = \pm 0.5$. Both solitons have equal norms, $N = 3$, the chemical potentials being $\mu_a = 1.71$ and $\mu_b = 2.08$, respectively. (c) A stable skew-asymmetric dipole soliton with parameters $(N, \Omega, H, g, \gamma) = (10, 1, 1, 0.3, 0.5)$. Note that a fundamental soliton with the same parameters as in (a) is unstable, as per Fig. 4(b).

C. Solitons' mobility

Generation of moving solitons from the quiescent ones considered above is a nontrivial problem, as Eq. (1), obviously, is not Galilean invariant. To this end, we rewrite the equations in the reference frame moving with velocity v , cf. Ref. [26]:

$$\begin{aligned}
 i\partial_t\phi_+ - iv\partial_\xi\phi_+ &= \partial_\xi\phi_- - \Omega\phi_+ - H\phi_- - g|\phi_+|^2\phi_+ + \frac{\gamma}{2}\phi_- \int_{-\infty}^{+\infty} |\xi - \xi'| \phi_-^*(\xi')\phi_+(\xi') d\xi', \\
 i\partial_t\phi_- - iv\partial_\xi\phi_- &= -\partial_\xi\phi_+ + \Omega\phi_- - H\phi_+ - g|\phi_-|^2\phi_- + \frac{\gamma}{2}\phi_+ \int_{-\infty}^{+\infty} |\xi - \xi'| \phi_-(\xi')\phi_+^*(\xi') d\xi',
 \end{aligned} \tag{12}$$

where $\xi \equiv x - vt$ is the moving coordinate. In this reference frame, stationary solutions are looked for as $\phi_\pm = \exp(-i\mu t) u_\pm(\xi)$, with complex stationary wave function u_\pm satisfying equations

$$\begin{aligned}
 \mu u_+ - iv\partial_\xi u_+ &= \partial_\xi u_- - \Omega u_+ - H u_- - g|u_+|^2 u_+ + \frac{\gamma}{2} u_- \int_{-\infty}^{+\infty} |\xi - \xi'| u_-^*(\xi') u_+(\xi') d\xi', \\
 \mu u_- - iv\partial_\xi u_- &= -\partial_\xi u_+ + \Omega u_- - H u_+ - g|u_-|^2 u_- + \frac{\gamma}{2} u_+ \int_{-\infty}^{+\infty} |\xi - \xi'| u_-(\xi') u_+^*(\xi') d\xi'.
 \end{aligned} \tag{13}$$

Note that, in the absence of the ZS ($\Omega = 0$), solutions of Eq. (13) satisfy the skew-symmetry condition generalized for the complex wave functions: $u_+(\xi) = \pm u_-^*(-\xi)$, cf. Eq. (4).

In the asymptotic area of $|\xi| \rightarrow \infty$, Eq. (13) takes the form of

$$\begin{aligned}\mu u_+ - iv\partial_\xi u_+ &= \partial_\xi u_- - \Omega u_+ - H u_- + \frac{\gamma}{2}\tilde{I}|\xi|u_-, \\ \mu u_- - iv\partial_\xi u_- &= -\partial_\xi u_+ + \Omega u_- - H u_+ + \frac{\gamma}{2}\tilde{I}^*|\xi|u_+, \end{aligned} \quad (14)$$

where

$$\tilde{I} \equiv \int_{-\infty}^{+\infty} u_-^*(\xi)u_+(\xi)d\xi, \quad (15)$$

cf. Eq. (9). The analysis of Eq. (14) yields, in the lowest approximation, the Gaussian asymptotic profile of the moving soliton,

$$\{u_-(x), u_+(x)\} \sim \exp \left\{ -\frac{\sqrt{[\text{Re}(\tilde{I})]^2 - v^2|\tilde{I}|^2 - i\text{Im}(\tilde{I})\text{sgn}\xi}}{4(1-v^2)}\gamma\xi^2 \right\}, \quad (16)$$

cf. Eq. (11). The Gaussian tails of a stable skew-symmetric moving soliton are compared to their analytical counterparts, predicted by Eq. (16), in Fig. 7(b). Similar to their quiescent counterparts [cf. Fig. 7)], the moving solitons are approximated reasonably well by the Gaussian ansatz for the tails.

As it follows from Eq. (16), the moving solitons may exist for velocities falling below a certain critical value, which is determined by an implicit condition

$$v^2 < v_{\text{max}}^2 = [\text{Re}(\tilde{I})]^2 / |\tilde{I}|^2 < 1. \quad (17)$$

Obviously, Eq. (17), which is produced by the consideration of the asymptotic form of the solitons' tails, is an upper limit, but not a sufficient condition, for the existence of moving solitons. Indeed, numerical findings demonstrate that largest velocities, up to which the solitons can be found, are smaller than the value given by Eq. (17).

Numerical results for moving skew-symmetric solitons are summarized in the form of stability regions in the planes of (g, v) and (N, v) shown in Fig. 10 for $(\Omega, H) = (0, 1)$. The figure demonstrates that the stability regions shrink with the increase of both $|g|$ and N , the largest velocity admitting the stability being attained in the absence of the contact nonlinearity, $g = 0$. Note that the maximum velocity in Fig. 10(a) is ≈ 0.5 , being, indeed, smaller than the respective value $v_{\text{max}} \approx 0.84$, which is predicted by the upper limit given by Eq. (17).

A typical example of a skew-symmetric moving soliton (with velocity $v = 0.5$) near the stability boundary is shown in Fig. 11(a). Further, the motion of solitons with velocities $v = \pm 0.1$ is illustrated by the density plots displayed in Figs. 11(b,c). Finally, the availability of the solitons moving in opposite directions makes it possible to simulate collisions between them. A typical outcome of collisions is displayed in Fig. 11(d). Due to the effective nonlocality of the microwave-mediated coupling, the solitons commence interacting before coming in contact, similar to what is shown above in Fig. 6(c). After several collisions, the two solitons merge into a single one, at $t > 220$.

IV. CONCLUSION

This work demonstrates that the concept of gap solitons in two-component BECs with the kinetic energy negligible in comparison with the SOC (spin-orbit-coupling) and ZS (Zeeman-splitting) terms in the Hamiltonian may be applied to the system in which two atomic states are resonantly coupled by the microwave radiation, the feedback of the two-component atomic wave function on the microwave field being represented by the Poisson's equation (which is solved by means of the Green's function). The nonlocal interaction between the components, mediated by the radiation, drastically changes the concept of the linear spectrum, adding to it an effective nonlinear trapping potential $\sim |x|$, thus making the system non-linearizable. As a result, the system may create families of both gap and embedded solitons, a considerable part of which is stable (the gap tends to remain empty while embedded solitons exist). In the case when the system includes repulsive (or zero) contact nonlinearity, the stability of soliton families obeys the anti-Vakhitov-Kokolov criterion. The two-component solitons feature exact or approximate (broken) skew-symmetric shapes. In addition to ground-state fundamental solitons, which may feature a node in their shape, the system supports dipole solitons, whose stability area is broader than for their fundamental counterparts. The stability area is identified too for moving solitons, being limited by a largest values of the velocity, and collisions between moving solitons lead to merger into a single one, via a complex interaction.

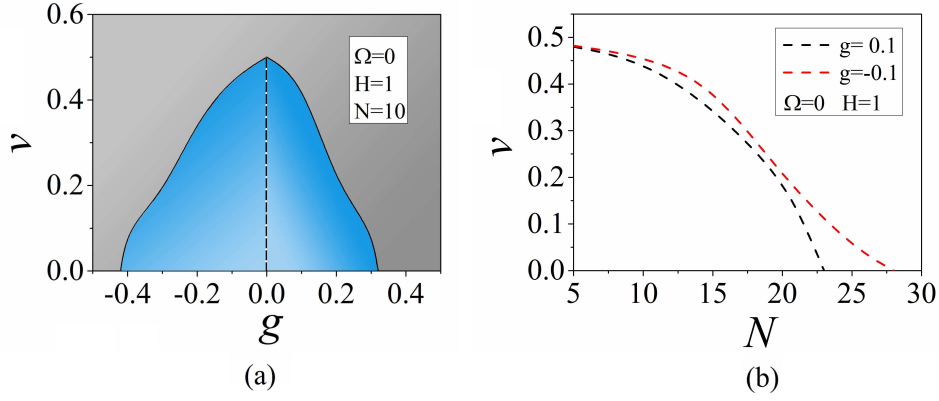


FIG. 10: Stability areas for skew-symmetric solitons moving with velocity v [blue in panel (a), and beneath the dashed boundaries in (b)], in parameter planes (g, v) and (N, v) . In panel(b), $g = -0.1$ corresponds to the red dashed line (upper). Values of other parameters are indicated in the panels.

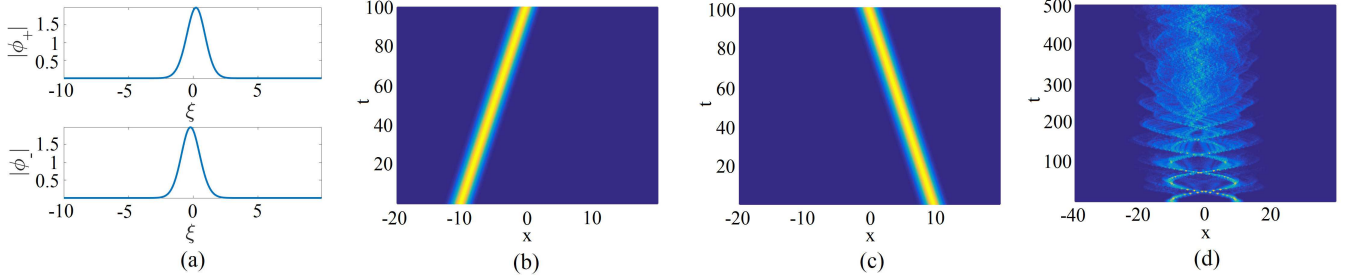


FIG. 11: (a) A moving skew-symmetric soliton located near the stability boundary, for $(N, H, \Omega, \gamma, g, v) = (10, 1, 0, 0.5, 0, 0.5)$. (b,c) Density plots for solitons moving with velocities $v = \pm 0.1$ are displayed in the quiescent reference frame, for parameters $(N, H, \Omega, \gamma, g) = (10, 1, 0, 0.5, 0)$. (d) Collision between solitons moving with opposite velocities, $v = \pm 0.1$.

A challenging problem for further analysis is the consideration of the two-dimensional version of the present system. In particular, the Green's function for the one-dimensional Poisson's equation should be replaced by its two-dimensional (logarithmic) counterpart [35].

Acknowledgment

This work is supported, in part, by the Israel Science Foundation through grant No. 1287/17, NNSFC (China) through Grants No. 11874112 and 11575063, and by the State Scholarship Fund of China Scholarship council through File No. 201808440001. Z. Fan appreciates technical assistance provided by Ms. Shiyue Liu (Chinese University of Hong Kong).

-
- [1] Y.-J. Lin, K. Jiménez-García, I. B. Spielman, Spin-orbit-coupled Bose-Einstein condensates, *Nature (London)*, **471**, 83 (2011).
[2] D. L. Campbell, G. Juzeliūnas, and I. B. Spielman, Realistic Rashba and Dresselhaus spin-orbit coupling for neutral atoms, *Phys. Rev. A* **84**, 025602 (2011).
[3] Y. Zhang, L. Mao, and C. Zhang, Mean-Field Dynamics of spin-orbit coupled Bose-Einstein condensates, *Phys. Rev. Lett.* **108**, 035302 (2012).
[4] Z. Wu, L. Zhang, W. Sun, X.-T. Xu, B.-Z. Wang, S.-C. Ji, Y. Deng, S. Chen, X.-J. Liu, and J.-W. Pan, Realization of two-dimensional spin-orbit coupling for Bose-Einstein condensates, *Science* **354**, 83-88 (2016).
[5] V. Galitski and I. B. Spielman, Spin-orbit coupling in quantum gases, *Nature* **494**, 49-54 (2013).
[6] H. Zhai, Degenerate quantum gases with spin-orbit coupling: a review, *Rep. Progr. Phys.* **78**, 026001 (2015).

- [7] S. Schulz, S. Schumacher, and G. Czycholl, Spin-orbit coupling and crystal-field splitting in the electronic and optical properties of nitride quantum dots with a wurtzite crystal structure, *Eur. Phys. J. B* **64**, 51-60 (2008).
- [8] I. A. Shelykh, A. V. Kavokin, Y. G. Rubo, T. C. W. Liew, and G. Malpuech, Polariton polarization-sensitive phenomena in planar semiconductor microcavities, *Semicond. Sci. Technol.* **25**, 013001 (2010).
- [9] V. G. Sala, D. D. Solnyshkov, I. Carusotto, T. Jacqmin, A. Lemaître, H. Terças, A. Nalitov, M. Abbarchi, E. Galopin, I. Sagnes, J. Bloch, G. Malpuech, and A. Amo, Spin-orbit coupling for photons and polaritons in microstructures, *Phys. Rev. X* **5**, 011034 (2015).
- [10] S. Dufferwiel, F. Li, E. Cancellieri, L. Giriunas, A. A. P. Trichet, D. M. Whittaker, P. M. Walker, F. Fras, E. Clarke, J. M. Smith, M. S. Skolnick, and D. N. Krizhanovskii, Spin textures of exciton-polaritons in a tunable microcavity with large TE-TM splitting, *Phys. Rev. Lett.* **115**, 246401 (2015).
- [11] K. Y. Bliokh, F. J. Rodriguez-Fortuno, F. Nori, and A. V. Zayats, Spin-orbit interactions of light, *Nature Photon.* **9**, 796-808 (2015).
- [12] Y. V. Kartashov and D. V. Skryabin, Modulational instability and solitary waves in polariton topological insulators, *Optica* **3**, 1228-1236 (2016).
- [13] O. Lafont, S. M. H. Luk, P. Lewandowski, N. H. Kwong, P. T. Leung, E. Galopin, A. Lemaître, J. Tignon, S. Schumacher, E. Baudin, and R. Binder, Controlling the optical spin Hall effect with light, *Appl. Phys. Lett.* **110**, 061108 (2017).
- [14] T. Kawakami, T. Mizushima, and K. Machida, Textures of $F = 2$ spinor Bose-Einstein condensates with spin-orbit coupling, *Phys. Rev. A* **84**, 011607(R) (2011).
- [15] H. Sakaguchi and B. Li, Vortex lattice solutions to the Gross-Pitaevskii equation with spin-orbit coupling in optical lattices, *Phys. Rev. A* **87**, 015602 (2013).
- [16] G. J. Conduit, Line of Dirac monopoles embedded in a Bose-Einstein condensate, *Phys. Rev. A* **86**, 021605(R) (2012).
- [17] C. J. Wu, I. Mondragon-Shem, and X.-F. Zhou, Unconventional Bose-Einstein condensations from spin-orbit coupling, *Chin. Phys. Lett.* **28**, 097102 (2011).
- [18] T. Kawakami, T. Mizushima, M. Nitta, and K. Machida, Stable skyrmions in $SU(2)$ gauged Bose-Einstein condensates, *Phys. Rev. Lett.* **109**, 015301 (2012).
- [19] O. Fialko, J. Brand, and U. Zülicke, Soliton magnetization dynamics in spin-orbit-coupled Bose-Einstein condensates, *Phys. Rev. A* **85**, 051605(R) (2012).
- [20] Y. Xu, Y. Zhang, and B. Wu, Bright solitons in spin-orbit-coupled Bose-Einstein condensates, *Phys. Rev. A* **87**, 013614 (2013).
- [21] V. Achilleos, D. J. Frantzeskakis, P. G. Kevrekidis, and D. E. Pelinovsky, Matter-wave bright solitons in spin-orbit coupled Bose-Einstein condensates, *Phys. Rev. Lett.* **110**, 264101 (2013).
- [22] Y. V. Kartashov, V. V. Konotop, and F. Kh. Abdullaev, Gap Solitons in a Spin-Orbit-Coupled Bose-Einstein Condensate, *Phys. Rev. Lett.* **111**, 060402 (2013).
- [23] L. Salasnich and B. A. Malomed, Localized modes in dense repulsive and attractive Bose-Einstein condensates with spin-orbit and Rabi couplings, *Phys. Rev. A* **87**, 063625 (2013).
- [24] L. Wen, Q. Sun, Y. Chen, D.-S. Wang, J. Hu, H. Chen, W.-M. Liu, G. Juzeliūnas, B. A. Malomed, and A.-C. Ji, Motion of solitons in one-dimensional spin-orbit-coupled Bose-Einstein condensates, *Phys. Rev. A* **94**, 061602(R) (2016).
- [25] Y. V. Kartashov and V. V. Konotop, Solitons in Bose-Einstein condensates with helicoidal spin-orbit coupling, *Phys. Rev. Lett.* **118**, 190401 (2017).
- [26] H. Sakaguchi, B. Li, and B. A. Malomed, Creation of two-dimensional composite solitons in spin-orbit-coupled self-attractive Bose-Einstein condensates in free space, *Phys. Rev. E* **89**, 032920 (2014).
- [27] V. E. Lobanov, Y. V. Kartashov, and V. V. Konotop, Fundamental, multipole, and half-vortex gap solitons in spin-orbit coupled Bose-Einstein condensates, *Phys. Rev. Lett.* **112**, 180403 (2014).
- [28] L. Salasnich, W. B. Cardoso, and B. A. Malomed, Localized modes in quasi-two-dimensional Bose-Einstein condensates with spin-orbit and Rabi couplings, *Phys. Rev. A* **90**, 033629 (2014).
- [29] H. Sakaguchi, E. Y. Sherman, and B. A. Malomed, Vortex solitons in two-dimensional spin-orbit coupled Bose-Einstein condensates: Effects of the Rashba-Dresselhaus coupling and the Zeeman splitting, *Phys. Rev. E* **94**, 032202 (2016).
- [30] Y. Li, Y. Liu, Z. Fan, W. Pang, S. Fu, and B. A. Malomed, Two-dimensional dipolar gap solitons in free space with spin-orbit coupling, *Phys. Rev. A* **95**, 063613 (2017).
- [31] H. Sakaguchi and B. A. Malomed, Flipping-shuttle oscillations of bright one- and two-dimensional solitons in spin-orbit-coupled Bose-Einstein condensates with Rabi mixing, *Phys. Rev. A* **96**, 043620 (2017).
- [32] Y.-C. Zhang, Z.-W. Zhou, B. A. Malomed, and H. Pu, Stable solitons in three-dimensional free space without the ground state: Self-trapped Bose-Einstein condensates with spin-orbit coupling, *Phys. Rev. Lett.* **115**, 253902 (2015).
- [33] B. A. Malomed, Creating solitons by means of spin-orbit coupling, *EPL* **122**, 36001 (2018).
- [34] D. L. Campbell, G. Juzeliūnas, and I. B. Spielman, Realistic Rashba and Dresselhaus spin-orbit coupling for neutral atoms, *Phys. Rev. A* **84**, 025602 (2011).
- [35] J. Qin, Z. Liang, B. A. Malomed, and G. Dong, Tail-free self-accelerating solitons and vortices, *Phys. Rev. A* **99**, 023610 (2019).
- [36] L. Salasnich and B. A. Malomed, Localized modes in dense repulsive and attractive Bose-Einstein condensates with spin-orbit and Rabi couplings, *Phys. Rev. A* **87**, 063625 (2013).
- [37] W. B. Cardoso and R. M. P. Teixeira, Scattering of solitons in binary Bose-Einstein condensates with spin-orbit and Rabi couplings, *Nonlin. Dynamics* **96**, 1147-1167 (2019).
- [38] A. Tononi, Y. Wang, and L. Salasnich, Quantum solitons in spin-orbit-coupled Bose-Bose mixtures, *Phys. Rev. A* **99**, 063618 (2019).

- [39] O. V. Borovkova, Y. V. Kartashov, L. Torner, and B. A. Malomed, Bright solitons from defocusing nonlinearities, *Phys. Rev. E* **84**, 035602 (R) (2011).
- [40] A. B. Aceves and S. Wabnitz, Self-induced transparency solitons in nonlinear refractive periodic media, *Phys. Lett. A* **141**, 37-42 (1989).
- [41] D. N. Christodoulides and R. I. Joseph, Slow Bragg solitons in nonlinear periodic structures, *Phys. Rev. Lett.* **62**, 1746-1748 (1989).
- [42] C. M. de Sterke and J. E. Sipe, Gap solitons, *Progr. Optics* **33**, 203-260 (1994).
- [43] B. J. Eggleton, R. E. Slusher, C. M. de Sterke, P. A. Krug, and J. E. Sipe, Bragg Grating solitons, *Phys. Rev. Lett.* **76**, 1627-1630 (1996).
- [44] J. T. Mok, C. Martijn de Sterke, I. C. M. Littler, and B. J. Eggleton, Dispersionless slow light using gap solitons, *Nature Phys.* **2**, 775-780 (2006).
- [45] E. A. Cerda-Méndez, D. Sarkar, D. N. Krizhanovskii, S. S. Gavrilov, K. Biermann, M. S. Skolnick, and P. V. Santos, Exciton-polariton gap solitons in two-dimensional lattices, *Phys. Rev. Lett.* **111**, 146401 (2013).
- [46] E. A. Ostrovskaya, J. Abdullaev, M. D. Fraser, A. S. Desyatnikov, and Yu. S. Kivshar, Self-localization of polariton condensates in periodic potentials, *Phys. Rev. Lett.* **110**, 170407 (2013).
- [47] V. A. Brazhnyi and V. V. Konotop, Theory of nonlinear matter waves in optical lattices, *Mod. Phys. Lett. B* **18**, 627 (1994).
- [48] O. Morsch and M. Oberthaler, Dynamics of Bose-Einstein condensates in optical lattices, *Rev. Mod. Phys.* **78**, 179 (2006).
- [49] B. Eiermann, T. Anker, M. Albiez, M. Taglieber, P. Treutlein, K. P. Marzlin, and M. K. Oberthaler, Bright Bose-Einstein gap solitons of atoms with repulsive interaction, *Phys. Rev. Lett.* **92**, 230401 (2004).
- [50] H.-Y. Hui, Y. Zhang, C. Zhang, and V. W. Scarola, Superfluidity in the absence of kinetics in spin-orbit-coupled optical lattices, *Phys. Rev. A* **95**, 033603 (2017).
- [51] J. Qin, G. Dong, and B. A. Malomed, Hybrid matter-wave-microwave solitons produced by the local-field effect, *Phys. Rev. Lett.* **115**, 023901 (2015).
- [52] Ye. Larionova, W. Stolz, and C. O. Weiss, Optical bistability and spatial resonator solitons based on exciton-polariton nonlinearity, *Opt. Lett.* **33**, 321-323 (2008).
- [53] A. R. Champneys, B. A. Malomed, J. Yang, and D. J. Kaup, “Embedded solitons”: solitary waves in resonance with the linear spectrum, *Physica D* **152-153**, 340-354 (2001).
- [54] J. K. Yang, Stable embedded solitons, *Phys. Rev. Lett.* **91**, 143903 (2003).
- [55] X. S. Wang, Z. G. Chen, J. D. Wang, and J. K. Yang, Observation of in-band lattice solitons, *Phys. Rev. Lett.* **99**, 243901 (2007).
- [56] D. Leykam and Y. D. Chong, Edge solitons in nonlinear-photonic topological insulators, *Phys. Rev. Lett.* **117**, 143901 (2016).
- [57] H. Sakaguchi and B. A. Malomed, One- and two-dimensional gap solitons in spin-orbit-coupled systems with Zeeman splitting, *Phys. Rev. A* **97**, 013607 (2018).
- [58] J. Yang, *Nonlinear waves in integrable and nonintegrable systems*, SIAM: Philadelphia, (2010).
- [59] N. G. Vakhitov and A. A. Kolokolov, Stationary solutions of the wave equation in a medium with nonlinearity saturation, *Radiophys. Quantum Electron.* **16**, 783-789 (1973).
- [60] L. Bergé, Wave collapse in physics: principles and applications to light and plasma waves, *Phys. Rep.* **303**, 259-370 (1998).
- [61] H. Sakaguchi and B. A. Malomed, Solitons in combined linear and nonlinear lattice potentials, *Phys. Rev. A* **81**, 013624 (2010).